Available online at www.sciencedirect.com
SCIENCE DIRECT
Journal of Magnetic Resonance 178 (2006) 193–205
JMR Journal of Magnetic Resonance
www.elsevier.com/locate/jmr

Motional relativity and industrial NMR sensors

B.P. Hills *, K.M. Wright

Institute of Food Research, Norwich Research Park, Colney, Norwich NR4 7UA, UK

Received 20 July 2005; revised 23 September 2005
Available online 24 October 2005

Abstract

We explore the implications of motional relativity in NMR and show that sample translation can be used to acquire NMR signals without the need for pulsed RF excitation or pulsed magnetic field gradients. Novel single-shot, on-line NMR acquisition protocols for samples being conveyed at high speed are discussed and preliminary results using a low-cost, on-line prototype NMR sensor are presented.

Keywords: Motional relativity; On-line NMR; Low-field NMR; Inhomogeneous fields; Quality control; Industrial sensor

1. Introduction

NMR has been widely exploited for clinical diagnosis in hospitals and as a research tool in analytical laboratories but apart from relatively minor off-line quality control applications it has failed to be developed as an on-line sensor in the industrial sector. This is surprising because almost every other type of spectroscopy, from Near Infra Red to X-rays, has been exploited as an on-line sensor to examine objects moving continuously, at speeds of several meters per second, on industrial conveyors [1]. There are several reasons often cited for this failure, namely

(a) NMR is too expensive because it requires expensive gradient and RF amplifiers and controllers and is usually based around super-conducting magnet technology.
(b) NMR is too delicate for a factory environment because it requires high magnetic field homogeneity and signal/noise is generally low.
(c) NMR is too slow for industrial conveyors moving at typical speeds of 2 m/s because the available acquisition time for moving samples is reduced to just a few tens of milliseconds.
(d) There is insufficient time to polarise samples characterised by T_1's in excess of a second moving at conveyor velocities, because samples need to travel a distance $5T_1v$ for complete polarisation. With a conveyor velocity, v, of 2 m/s and a typical T_1 of 1 s this amounts to 10 m, which is impractical.
(e) NMR requires highly skilled (and expensive) operators and technical support.

These are valid criticisms, but they are based on current NMR protocols. In this paper, we show how the principle of "motional relativity" which uses the movement of the sample itself to modify, or even create, NMR signals can, in principle, overcome these objections.

The commercial potential for low-cost NMR sensors in the manufacturing sector is enormous. Food manufacturing is the largest industrial sector and many NMR papers have shown the existence of useful correlations between NMR parameters and food quality and these can, potentially, be developed into on-line quality control protocols. NMR studies of quality defects in horticultural products (fruit, vegetables, and bulbs) have been reviewed [2] and reveal numerous potential applications including the detection of bruising, infection and physiological defects induced by over-ripening or long-term storage. Foreign body detection in processed food is another area ripe for

* Corresponding author. Fax: +44 01603 507723.
E-mail address: brian.hills@bbsrc.ac.uk (B.P. Hills).

1090-7807/$ - see front matter © 2005 Elsevier Inc. All rights reserved.
doi:10.1016/j.jmr.2005.09.010

exploitation. Bone fragments in processed meat and fish as well as metal, glass, and plastic foreign bodies introduced during manufacture are a constant concern in the food industry. Existing dual X-ray sensors are expensive and are only able to detect foreign bodies containing atoms with high X-ray scattering cross-sections such as the calcium in bone fragments. Pieces of plastic, insects, wooden splinters, and other organic objects therefore pass undetected through X-ray scanners. This, in principle, is not a limitation with an on-line MRI foreign body detector, though low signal/noise might limit detection sensitivity. Besides foreign body detection there are a host of quality concerns related to the oil, fat, and water content of processed meat, fish, dairy, egg, and cereal products. This includes spoilage changes such as creaming and undesired phase separations. Process control is another area where NMR sensors could make a significant impact. In process control the spatial aspect of imaging is not really needed and an on-line NMR sensor could continuously and non-invasively monitor the composition and/or viscosity and/or temperature of continuously extruded or pumped semi-solid material. Such monitoring relies on the dependence of the NMR relaxation times and signal amplitudes on the processing variables. Space does not permit discussion of the numerous potential applications of an on-line NMR sensor in other industrial sectors such as the pharmaceutical, construction, and oil industries. Suffice it to say that there is considerable incentive to overcome the problems listed earlier and transfer NMR and MRI technology out of the laboratory and into the factory. To achieve this objective first requires consideration of the motional relativity principle in spin physics because this has the potential of removing the need for expensive RF and gradient controllers or even of high field homogeneity that characterises conventional NMR.

2. The motional relativity principle in NMR

In this section, we explore the possibilities for performing NMR using only constant (i.e., non-pulsed) magnetic and radiofrequency fields and where sample translation is used to create a time-dependent signal. We begin with the radiofrequency excitation step.

2.1. Motional relativity and radiofrequency excitation

In conventional NMR an on-resonance RF pulse of time-dependent amplitude, $B_1(t)$, tips the longitudinal magnetisation vector in a polarised sample through an angle, θ, in the rotating frame, such that

$$\theta = \int \mathrm{d}t\,\gamma B_1(t). \tag{1}$$

An alternative way of achieving the same result, which exploits motional relativity, is to set up a localised region of space containing a spatially characterized, time-invariant, continuous radiofrequency field, B_1, which is transverse to the main magnetic field, B_0. The excitation is then achieved by translation of the sample through this localised volume of RF radiation. The tip angle θ, in the on-resonance rotating frame for a spin moving in one dimension (along the z-axis) through an on-resonance RF field, $B_1(z)$, is then given by the integral

$$\theta = \int \mathrm{d}t\,\gamma B_1(t) = \int \mathrm{d}z\,(\mathrm{d}t/\mathrm{d}z)\gamma B_1(z). \tag{2}$$

For a sample entering the region with initial velocity u and acceleration, a,

$$z = ut + at^2/2 \tag{3}$$

so that time can be replaced by distance as a variable such that,

$$\theta = \int \mathrm{d}z\,\gamma B_1(z)/[u^2 + 2az]^{1/2}. \tag{4}$$

There are major advantages with this alternative excitation protocol in on-line situations. First, rapid translation of the sample through the RF field at velocities of several meters per second no longer requires extended regions of radiofrequency B_1 homogeneity along the direction of motion. Even quite inhomogeneous radiofrequency fields are effective because only the spatial integral of the RF field enters Eq. (4). Second, because the RF irradiation is continuous there is no need for expensive RF pulse programmers. Third, because the RF field is no longer pulsed there are no induced eddy currents or associated coil ring-down phenomena. Eq. (4) also shows that there is no reason to be restricted to samples moving at constant velocities. Accelerating samples, such as powders falling under gravity through the RF coil, can be excited in the same way. This excitation mode, which we call the "ST" mode (for sample translation) is especially suited to simple on-line applications requiring only one or two excitation pulses. As we shall show, on-line multi-pulse sequences are best implemented with conventional pulsed RF methods.

2.2. Motional relativity and signal acquisition

In the ST excitation mode, the FID of the spins emerging from a region of constant radiofrequency excitation will differ from the FID of a pulsed RF experiment on a stationary sample because spins at different locations in a finite-sized sample emerge from the RF field at different times and therefore end up with different phases due to free precession in the main field, B_0. In the following, we define zero time as the instant the whole sample emerges from the RF excitation region. Neglecting relaxation, the signal, dS, from a volume element (a slice) located at z at time t in the laboratory frame is

$$dS(z,t) = \rho(z)\cdot\exp[\mathrm{i}\varphi(z,t)]\,\mathrm{d}z, \tag{5}$$

where $\rho(z)$ is the local slice transverse magnetisation density and $\varphi(z,t)$ is the phase. In the laboratory frame, $\varphi(z,t) = (\varphi_0 + \omega_0 t)$ where the initial phase distribution,

$\varphi_0(z)$, is, neglecting acceleration, $\omega_0(z/v)$. The total signal is therefore

$$S(t) = \exp(\mathrm{i}\omega_0 t) \int \mathrm{d}z \rho(z) \exp[\mathrm{i}\omega_0(z/v)]. \quad (6)$$

This is a Fourier transform with a fixed wavevector, $k_0 = \omega_0/v$, which should be contrasted with the conventional FID on a stationary sample in a pulsed RF experiment, which is $S(k_0 = 0, t)$. This, k_0 "phase twist" through the sample is the same as would be obtained on a stationary sample by a hard 90° pulse followed immediately by a pulsed gradient, G_z, of duration δ such that $\gamma G_z \delta = k_0 = \omega_0/v$, which is the first part of a PGSE experiment. This suggests that a spin echo can be created by motion of the sample through a second region of continuous RF irradiation of an intensity and length sufficient to give a 180° pulse and located a distance vT further down the track. The magnetisation at a position z inside the sample immediately before it enters the 180° RF region at a time T after emergence from the 90° RF region is

$$dS(z,t) = \rho(z) \exp[\mathrm{i}k_0 z + \mathrm{i}\omega_0 T]. \quad (7)$$

The magnetisation after the sample emerges from the 180° region is obtained by taking the complex conjugate of (7) and multiplying by a second phase factor $\exp(\mathrm{i}k_0 z)$ due to the finite sample size which eliminates the phase twist wavevector, k_0. The remaining factor $\exp(-\mathrm{i}\omega_0 T)$ is eliminated after an additional evolution time T after the sample emerges from the 180° RF region. The net result, in the absence of relaxation and diffusion, is a spin echo of amplitude $\rho(z)$ at a distance $2vT$ from the first 90° RF region. This derivation does, however, assume that the B_0 field is perfectly homogeneous over the distance $2vT$ between the first RF coil and the spin echo. Unfortunately this is unlikely to be the case and dephasing caused by the field inhomogeneities experienced by sample translation along the track will not, in general, be refocused by the 180° pulse. This attenuation process, which we call "translational dephasing," differs from conventional T_2, T_2^* or diffusive processes because each spin experiences a unique path in time-frequency space as it moves down the track depending on its position within the sample and the z-dependence of the external field inhomogeneity at that position. In general the inhomogeneity will not be the same before and after the 180° excitation so refocusing will be imperfect or non-existent. The best way to avoid such "translational dephasing" is to store the magnetisation as longitudinal magnetisation for passage between RF coils with a suitable flip-back pulse performed either in the ST- or pulsed RF mode.

The emergence of the Fourier transform in Eq. (6) suggests that image profiling is possible if we impose a constant, time-invariant field gradient, G, oriented along the direction of sample motion. An analogous derivation shows that in this case,

$$\varphi(z,t) = (\omega_0 + \gamma G z)z/v + \omega_0 t + \gamma G z t + \tfrac{1}{2}\gamma G v t^2 \quad (8)$$

and the Fourier transform relationship is now,

$$S(t) = \exp[\mathrm{i}\omega_0 t] \cdot \exp\left[\mathrm{i}\frac{1}{2}\gamma G v t^2\right] \cdot \int \mathrm{d}z \rho(z) \exp[\mathrm{i}(k_0 + k)z] \cdot \exp[\mathrm{i}\gamma(G/v)z^2]. \quad (9)$$

Here, the wavevector k is defined in the usual way as $\gamma G t$. Providing $\gamma G/v$ is very small (the weak gradient, high velocity approximation) we can neglect the term in z^2 which prevents inverse Fourier transformation. The preexponential factor $\exp[\mathrm{i}\omega_0 t]$ can also be set to unity if we perform the experiment "on-resonance," in which case

$$S(t) = \exp\left[\mathrm{i}\frac{1}{2}\gamma G v t^2\right] \cdot \int \mathrm{d}z \rho(z) \exp[\mathrm{i}(k_0 + k)z]. \quad (10)$$

Eq. (10) shows that the image, $\rho(z)$, is obtained as the inverse Fourier transform of $S(t)\exp[-\mathrm{i}\frac{1}{2}\gamma G v t^2]$ except that the k_0 wavevector introduces a constant offset in k-space. Note especially that in this one-dimensional ST-mode imaging experiment all fields are time-invariant and only the sample moves so that expensive gradient amplifiers and controllers are no longer necessary and the RF is continuous, not pulsed. Because the gradient, G, is not pulsed there is, in fact, no need for a separate linear gradient coil. Instead the linear gradient, G, can be regarded as the first term in a Taylor expansion of the local B_0 field inhomogeneity over a region extending for a sample length from the RF coil. In other words, the main field, B_0, is deliberately made locally inhomogeneous to first order, so as to obtain an image. This runs counter to the conventional NMR wisdom based on stationary samples where B_0 homogeneity is paramount. The above derivation can, of course, be generalised to include spin echoes by inclusion of a second 180° excitation region, accelerating samples and higher-order non-linear field gradient terms and provides the basis for a variety of novel on-line imaging protocols. The development of a flow sensor for fluids based on non-pulsed gradients can also be considered and this contrasts with conventional flow imaging which phase-encodes the flow with bipolar gradient pulses [9].

The motional relativity principle is trivially simple for gradients transverse to the direction of sample motion because the vector product $\mathbf{G} \cdot \mathbf{v}$ is then zero so the signal is not motionally modulated. Passage through a spatially localised time-invariant transverse gradient is therefore exactly equivalent to applying a pulsed transverse gradient to a stationary sample. This means that two-dimensional back-projection imaging could, in principle, be done without any gradient pulsing by translating the sample through a set of permanent m-transverse gradients equally spaced along the track and oriented at an angle ϕ to the vertical such that $\phi = 0, \pi/m, 2\pi/m, \ldots, \pi$ and acquiring a spin echo in each gradient.

There are clearly a number of different ways for developing a low-cost, on-line NMR sensor based on motional relativity. Most conventional pulse sequences can be transposed, at least on paper, into the ST mode with arrays of constant gradients and RF sources arranged along the conveyor track. However, in many cases the arrays would

be impractical to construct and implement. Therefore, our approach in what follows is to first research the principle of motional relativity by translating the sample through constant (i.e., non-pulsed) gradients but with conventional pulsed RF excitation. If the constant gradient protocols are successful an attempt can be made at a later stage to replace the pulsed RF mode with the lower cost ST excitation mode or even with an RF-free mode. This approach has the advantage that multipulse sequences can be researched with the RF mode that may not be practical to implement in the ST mode. The pulsed RF mode corresponds to the $k_0 = 0$ limit in Eq. (10) and is therefore the basis of what follows. For the same reason, we have used separate gradient coils so that the magnitude of the gradients can be varied, even though they are not pulsed. Once the gradient strength and shape has been optimised for any particular application, the same gradient can, at a later stage, be incorporated into the B_0 field by, for example, introducing non-uniform coil winding in a main-field solenoid coil.

2.3. Motional relativity and coil design

To exploit motional relativity and maximize signal acquisition times with samples moving at several meters per second all RF, B_0, shim and gradient coils have had to be redesigned as cylindrical modules that can be wrapped around the conveyor and extended to arbitrary lengths along the direction of sample motion. At the same time it is essential to maintain commercial viability by keeping all costs to a minimum. For this reason a prototype sensor has been built using a long (1.7 m) air-cooled solenoid electromagnet (see Fig. 1). Air cooling rather than water-cooling was chosen because of its greater simplicity and lower cost. However, the need to keep the air-cooled magnet at a reasonable temperature, below ca. 60 °C at its hottest part, sets an upper limit on the current and therefore field strength in the system. Higher fields and higher currents give better signal/noise so there is a major advantage in using multiple independent concentric solenoid coils each powered by independent constant-current sources rather than a single coil. This follows because the heat generated in a solenoid coil is proportional to the square of the current; whereas the magnetic field is proportional to the current itself, so the same field can be achieved with roughly $(1/n)$ of the current through each of n coils and $(1/n)$ times less total heat output compared with a single coil of the same wire length. The increased surface area created by air gaps between the concentric coils also improves cooling efficiency. Our prototype therefore uses two concentric solenoids. The inner one has inner and outer diameters of 21.0 and 28.7 cm; whereas the outer solenoid has inner and outer diameters of 30.9 and 38.6 cm, and this gives a 1 cm air-gap between them. To channel the air more efficiently the outer surface of the outer coil is also surrounded by a 1 cm air gap and plastic ducting is used to force the air through the magnet gaps. As illustrated in Fig. 1 two industrial grade fans are used to both blow and extract the air through the magnet and this arrangement permits a field of ca. 0.06 T (corresponding to a proton frequency of ca. 2.55 MHz) to be achieved with the steady-state magnet temperature below 50 °C using only room-temperature (22 °C) air for cooling. Because of the forced air cooling the temperature–time curve at any point in the coil after the power supply is switched on follows Newtons law such that, $\theta(t) = \theta(\infty) - (f/c)\exp(-ct)$, where f is proportional to the rate of heat production and c is a heat transfer coefficient. Measurement of f and c for a given current therefore permits optimisation of the magnet system. To ensure safe operation in an industrial context the prototype has sensors continuously monitoring the power supplies to each solenoid coil and to the two cooling fans as well as the magnet temperature and air flow rate. If abnormal readings are reported the whole system is automatically shut down by a Eurotherm controller in programmed steps designed to avoid high induced back-voltages that could damage the electronics. Surge protectors have also been introduced between the power supplies and magnet for the same reason. Despite their need for a power supply and efficient cooling, solenoid magnets have major advantages over permanent magnet arrangements because the field strength can be easily varied and stabilised using a constant current power supply and the field

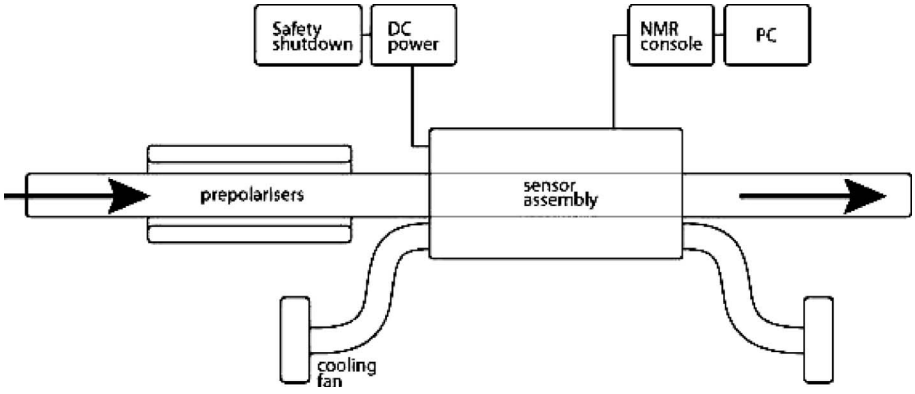

Fig. 1. Schematic of the low-cost, on-line NMR sensor prototype based on an air-cooled solenoid electromagnet and permanent magnet prepolarisers.

homogeneity in a long solenoid is sufficiently high to permit NMR even without shim coils. Even so, we have shimmed the B_0 field to order z^3 with home-made concentric, cylindrical z and z^2 shim coils located inside the inner solenoid magnet and extending along its whole length and these reduce the linewidth of a 10 cm long water phantom at the centre of the coil to about 150 Hz. These additional coils comprise copper wire wound in groves cut in plastic formers at variable spacing calculated to give linear and quadratic field profiles over the 1.7 m length of the solenoid magnet. Here also a 1 cm gap between the outer z^2 and inner z gradient coils ensures efficient air cooling. As already mentioned, in any commercial version the constant current z- and z^2 coils could be incorporated into the main solenoid magnet by varying the solenoid winding density.

It is worth noting that the design of the on-line linear gradient coil differs from the linear z-gradient coil in conventional spectrometers in that the winding direction is not reversed in the coil centre and the turn density does not increase linearly in either direction from the coil centre. This conventional ''reverse direction'' winding is desirable when stationary samples are examined in the centre of the coil because it means that increasing the gradient strength does not shift the resonance frequency at the coil centre. However, in on-line applications the sample travels the whole length of the coil so it is important that the field increases from zero at the point of entry to a maximum on exit. In this way the sample does not experience a region of large field inhomogeneity caused by the drop off in end-gradients as it enters the coil. We therefore use a coil winding curve, $\theta(z)$, such that the winding density increases linearly with z along the whole length of the coil. In other words, $\mathrm{d}\theta/\mathrm{d}z$ is proportional to z, where we have used cylindrical coordinates (z,θ) to specify the coil position on the cylinder surface. Integration with the boundary conditions $(z=0,\theta=0)$ and $(z=L,\theta=2\pi N)$ gives

$$z = L\{[(\theta+b)^{0.5} - b^{0.5}]/[(2\pi N+b)^{0.5} - b^{0.5}]\}. \quad (11)$$

Here, N is the total number of turns along the cylinder of length L and b is a parameter determining the initial number of windings at $z=0$, with $b=1$ giving the optimum gradient profile. A novel extendible transverse gradient coil wound on a cylindrical former has also been designed for use in on-line diffusion and imaging applications (patent pending). The z^2 shim coil follows the conventional design with the winding density increasing from the centre in both directions so as to counter the drop in field intensity at the ends of the solenoid coils.

A special, low-cost, low-field, transverse RF coil with cylindrical symmetry was designed for the sensor. A simple solenoid RF coil could not be used because B_1 needs to be transverse to B_0. Saddle and birdcage coils give the desired transverse field but are more expensive and have limited B_1 homogeneity and long pulse durations. These difficulties can be overcome using a series-wound, eddy-compensated, tilted solenoid RF coil. This contains solenoid-like coils tilted at 45° and uses the induced currents in a set of concentric vertical inner ''free-floating'' coils to remove the undesired longitudinal B_1 field component. This design is similar to a parallel-wound tilted coil developed for extremity imaging [10] but it was necessary to shorten the pulse durations and decrease the resonance frequency using series rather than parallel winding. This follows because N parallel connected loops reduce the inductance by a factor of N^2 compared to a series winding, so the resonance frequency of a parallel winding is a factor of N times higher. Parallel winding also divides the current between the N loops, giving undesirably long pulse durations. The tilted solenoid design has the advantage of being extendable to arbitrary lengths limited only by the need to avoid destructive interference when the wire length approaches half the RF wavelength. The decreasing filling factor can also become a problem with extended coils. The prototype transverse RF coil fitted inside the linear z-gradient coil and had an internal diameter of 12 cm and a length of 34 cm and had 10 equally spaced tilted loops. It was driven by a 400 W power transmitter in a commercial Resonance Instruments UltraMaran NMR console which was adapted for operation at low frequency. Typical 90° pulse durations were 45 μs, with a deadtime of ca. 100 μs. External noise was reduced by wrapping the whole magnet with earthed copper foil and locating earthed low-pass filters between the power supplies and the solenoid coils. The filter width was also reduced during acquisition to remove several peaks arising from coherent noise.

In the prototype arrangement individual samples were dragged through the sensor on a plastic track at controlled velocities using a computer-controlled stepper-motor so it is necessary to synchronise the passage of the sample through the magnet with the start of the RF pulse sequence. This was done by placing a photogate light beam across the track just outside the entrance to the magnet so that when the sample cuts the beam it triggers a delayed pulse sequence in the RF coil. The time taken by the sample to move from the photogate to the most homogenous part of the RF coil was calibrated for each conveyor velocity by continuously and rapidly pulsing a driven equilibrium Fourier transform (DEFT, [12]) pulse sequence $(\theta_x\text{–}\tau\text{–}2\theta_y\text{–}\theta_{-x}\text{–}t_1)_n$ and observing the change in the steady-state signal when the sample passes through the RF coil. The signal amplitude is observed to pass through a maximum when the sample is located in the most homogeneous part of the B_1 field.

3. Prepolarisation and the adiabatic principle

The discussion in Sections 2.1 and 2.2 assumed that the sample is fully polarised (i.e., contains its equilibrium longitudinal magnetisation) before entering the RF excitation coil. This, however, is an unreasonable assumption for samples characterised by long T_1's such as high water content fruit. A sample with a T_1 of 1 s travelling at 2 m/s would need to travel 10 m ($5T_1v$) before it is fully polarised,

which requires an unreasonably long solenoid magnet. To circumvent this difficulty the prototype sensor was equipped with a prepolarising module (see Fig. 1). This contains low-cost rectangular ferrite permanent magnet blocks positioned either side of the conveyor track, creating a higher field (ca. 0.12 T) than that in the solenoid (0.06 T) and oriented transverse to the sample motion. Samples first pass through the prepolarising module before entering the main solenoid sensor field. The higher prepolarising field means that sufficiently high polarisation in the lower solenoid field can be achieved in a shorter distance. In fact samples with short T_1 are superpolarised relative to the solenoid field. Of course the required length of the prepolarising module will depend on the T_1 so it was constructed in modular units, each 30 cm long, that can be connected together in various numbers.

Two aspects of prepolarisation are noteworthy. The sample emerges from the prepolariser with longitudinal magnetisation oriented transverse to the direction of motion; whereas the solenoid magnet creates a B_0 field oriented parallel to the direction of motion. The sample polarisation therefore needs to be rotated through 90° before NMR is possible. However, simple mechanical rotation will not suffice because the sample necessarily travels through a region of highly inhomogeneous stray field in the gap between the prepolariser and the solenoid. On first consideration this would appear to prevent any coherent on-line NMR. Fortunately the adiabatic principle [3] rescues the situation and ensures that, in most circumstances, the magnetisation in each spin isochromat in the sample follows the changing orientation of its local external field, so that the magnetisation is realigned inside the solenoid magnet and NMR is still possible. For the same reason the sample can be mechanically rotated as it travels through the prepolariser to ensure a more uniform polarisation.

Of course, the adiabatic principle merely determines the rate of reorientation of the longitudinal magnetisation not its magnitude, which is determined by longitudinal relaxation. It is therefore noteworthy that longitudinal relaxation as samples travel through the prepolariser, gap, and solenoid magnet can be exploited to give a new type of image contrast, namely the degree of polarisation, P. This depends not only on the field-dependent longitudinal relaxation time, T_1 at the frequency $\gamma B_0(z)$, which varies along the track, but also on the changing asymptotic longitudinal magnetisation, $\chi B_0(z)$. The stray field in the gap between the prepolariser and the solenoid corresponds to low resonance frequencies, $\gamma B_0(z)$, of just a few tens of kHz so that $T_1\{\gamma B_0(z)\}$ in the gap differs significantly from its usual high-field value and needs to be measured with a field-cycling spectrometer. Because T_1 generally decreases with decreasing field strength in biological samples, polarisation contrast may offer greater sensitivity for distinguishing quality factors than high field T_1 measurements. Polarisation contrast can be varied in many ways, either by altering the length of the stray field gap or by changing the prepolariser length or even the prepolarising field strength by varying the separation, thickness, and type of ferrite or neodymium-ferrite block magnets used in the prepolariser. The relationship between polarisation contrast, $P(r)$, and sample quality factors is unknown for most applications and will need to be researched if commercial applications are to be optimised.

4. Single-shot on-line pulse sequences

Because each sample travels through the sensor only once there is no possibility of using conventional pulse sequences based on repeated acquisition and/or phase cycling. Instead maximum information must be extracted in a single passage through the sensor, which means it is necessary to develop novel single-shot on-line equivalents of the conventional pulse sequences for image profiling, T_2, T_1, self-diffusion (D) and solvent suppression.

4.1. Single-shot on-line T_2 measurements

On first consideration, on-line single-shot measurements of T_2 appear straightforward because the Hahn-echo and CPMG sequences can be operated without phase cycling or repeated acquisition. There are, however, potentially serious complications when implementing the CPMG sequence on-line. As discussed in Section 2.2, 180° pulses do not, in general refocus the dephasing caused by translational relaxation, and so any attempt to convey transverse magnetisation down the magnet between two RF coils is likely to fail unless the B_0 field is homogeneous over the whole distance between RF coils. It is therefore best to perform the CPMG sequence in a multipulse RF mode within a single (extended) RF coil. But even within a single RF coil there are other difficulties. The conventional CPMG spin-echo sequence on stationary samples automatically refocuses the dephasing effects of B_0 inhomogeneity but we cannot assume this will happen when the sample moves through different regions of an inhomogeneous B_0 solenoid field in its passage through the RF coil. Moreover, because of its finite size, the B_1 field in the RF coil is also inhomogeneous, so as the sample moves through the RF coil the B_1 field strength varies and the same RF pulse duration gives different tip angles in different parts of the coil. A pulse duration adjusted to give a 180° tip angle in the RF coil centre will not give the same tip angle in other parts of the coil, so that the net effect of a conventional CPMG sequence with trains of 180° pulses will depend on sample velocity and the z-dependence of the B_1 field. The problem is compounded with gross B_0 inhomogeneity if the RF coil is positioned off-centre in the solenoid field. This is a realistic situation in any commercial sensor because multiple RF coils positioned along the solenoid magnet would permit increased sample throughput and/or multiple NMR measurements on each sample.

We first examine the mechanism of translational relaxation in more detail by calculating the time-evolution of a

single spin isochromat. The inhomogeneity in the main B_0 field can be expanded as a Taylor series about some arbitrary position in the RF coil where a spin isochromat has a resonance offset, δ_0. Because of the local field gradient the resonance offset for the spin isochromat will increase linearly with time at a constant rate $\mathrm{d}\delta/\mathrm{d}t$ as the sample moves down the track. At a time τ after a hard 90_x pulse, the isochromat will have accumulated a phase, φ, given by:

$$\varphi = \pi/2 + \int_0^{\tau} \mathrm{d}t[\delta_0 + (\mathrm{d}\delta/\mathrm{d}t)t], \tag{12}$$

$$\varphi = \pi/2 + \tau\delta_0 + 0.5(\mathrm{d}\delta/\mathrm{d}t)\tau^2. \tag{13}$$

Immediately after a refocusing 180_y applied at a time, τ, the phase becomes,

$$\varphi = \pi/2 - \tau\delta_0 - 0.5(\mathrm{d}\delta/\mathrm{d}t)\tau^2. \tag{14}$$

After a further time τ,

$$\varphi = \pi/2 - \tau\delta_0 - 0.5(\mathrm{d}\delta/\mathrm{d}t)\tau^2 + \int_{\tau}^{2\tau} \mathrm{d}t[\delta_0 + (\mathrm{d}\delta/\mathrm{d}t)t], \tag{15}$$

$$\varphi = \pi/2 - \tau\delta_0 - 0.5(\mathrm{d}\delta/\mathrm{d}t)\tau^2 + \tau\delta_0 + 1.5(\mathrm{d}\delta/\mathrm{d}t)\tau^2, \tag{16}$$

$$\varphi = \pi/2 + (\mathrm{d}\delta/\mathrm{d}t)\tau^2. \tag{17}$$

The spin isochromat therefore experiences a second-order phase shift $(\mathrm{d}\delta/\mathrm{d}t)\tau^2$ at the echo time 2τ. If all the spins had this phase shift it could be removed by a simple magnitude operation. Unfortunately, because of B_0 field inhomogeneity in the RF coil, spin isochromats in different parts of the sample experience different values of $(\mathrm{d}\delta/\mathrm{d}t)$ so the second-order phase shifts from spins in different locations within the sample destructively interfere and this attenuation cannot be removed by a magnitude operation. This, in essence, is the mechanism of translational relaxation. Unfortunately there is an additional complication in that the above derivation assumes that all spins experienced an initial 90° pulse which will not, in general, be true for a finite-sized sample moving through an inhomogeneous B_1 field. Clearly, all this means that the apparent T_2 measured with the CPMG sequence in a single RF coil will depend on sample velocity, and at sufficiently high velocities, depending on the B_0 and B_1 field inhomogeneities, the measured "apparent T_2" will become less than the true sample T_2.

To calculate the magnitude of these effects in our prototype sensor a numerical simulation was undertaken which incorporates the effects of finite sample size, the B_0 and B_1 field inhomogeneities as well as RF coil position. This simulation is described in Appendix A and Fig. 2A shows the field inhomogeneity maps used as input. The B_0 field map has been calculated for our solenoid magnet, while a trapezoid B_1 profile mimics the measured B_1 field inhomogeneity of our RF coil reasonably well. Spherical sample geometry has been assumed, which gives the semi-ellipsoid profile seen in Fig. 2A. The bottom part of Fig. 2 shows representative simulated CPMG echo decay envelopes, in this case for spherical samples moving at the indicated

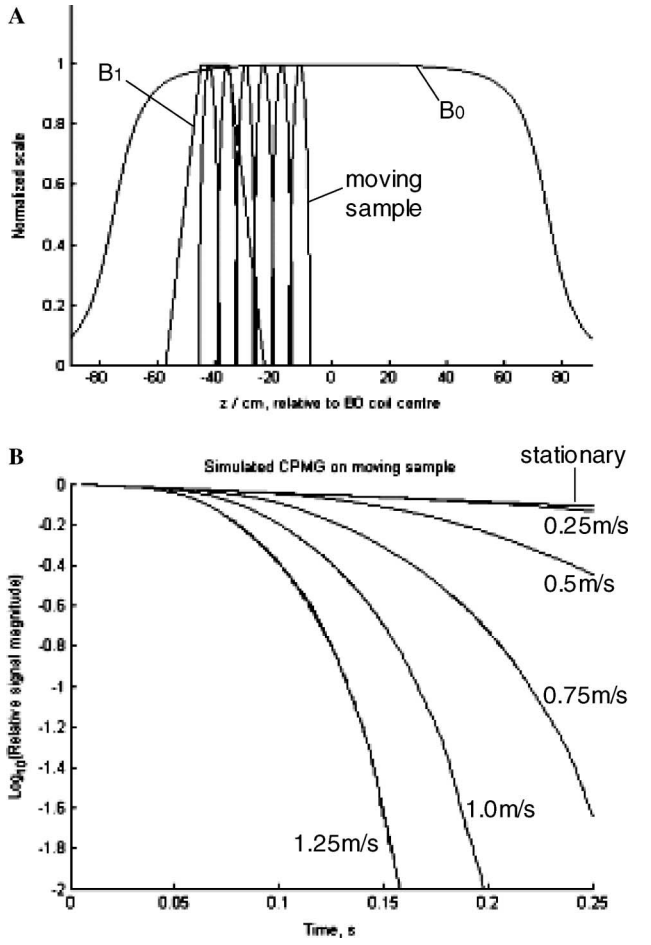

Fig. 2. (A) This shows the trapezoid B_1 of an off-centre RF coil, the B_0 map of the solenoid magnet and the semi-ellipsoidal profile of a spherical sample used in the simulation. (B) The calculated CPMG echo decay envelopes for the indicated sample velocities.

speeds through the trapezoid RF field located one-third of the way along the solenoid magnet. The simulation shows that when the RF coil is well off-centre it is only possible to determine meaningful T_2's out to acquisition times of about 40 ms with samples moving at 1.25 m/s. Fig. 2B also shows that if the sample velocity is reduced to 0.25 m/s it is possible to measure T_2's of several hundred milliseconds but there are few industrial situations where such low conveyor speeds would be economic. On a more positive note, there are, in principle, NMR strategies for improving the situation. For example, the simulation assumes that the echoes are generated by a train of 180° pulses of equal duration, so that, as the sample moves through the RF coil, the tip angle varies. In principle it is possible to adjust the duration of each pulse to compensate for the B_1 variation and thereby extend the duration of the true 180° pulse train. This would not compensate for the B_0 variation, but, as Eq. (17) shows, if radial inhomogeneity could be removed, all spins would experience the same second-order phase shift as they moved through the B_0

Table 1
A comparison of on-line CPMG T_2 measurements for a bottle of copper sulphate doped water moving at 1.25 m/s through a centred RF coil in the prototype sensor with those on the stationary sample

$CuSO_4$ concentration (M)	Static sample T_2 (ms)	T_2 of moving sample (ms)
0.1	5	5.2
0.03	17	15
0.01	54	41
0.003	169	42
0.001	453	84
0.0003	1091	75

For moving samples, T_2's longer than ca. 40 ms cannot be sensibly determined.

inhomogeneity along z, so this phase shift could be removed by a magnitude operation.

Table 1 shows our experimental CPMG results for a plastic bottle containing copper sulphate doped water with the indicated static T_2's and moving at 1.25 m/s. In this case all the refocusing pulses were of equal duration fixed at that for a 180° pulse at the centre of the RF coil and the RF coil was located in the centre of the solenoid magnet. It can be seen that even with the RF coil centrally located, sample motion at 1.25 m/s still sets an upper limit of about 40–50 ms for reliable T_2 measurements.

If more than one RF coil is located along the sample path then it will be necessary to avoid translational dephasing by storing transverse magnetisation as longitudinal magnetisation for passage between RF coils. This can be done with a single flip-back pulse with a duration appropriate for the sample position in the coil. Alternatively, if signal/noise permits, the initial 90° excitation pulse could be replaced by a smaller tip angle so that longitudinal magnetisation is reserved for use downstream.

4.2. On-line image profiling for foreign body detection

The protocol of Section 2.2 shows that a one-dimensional image profile can be obtained using a constant (non-switched) gradient oriented along the direction of motion provided the motionally modified spin echo is first multiplied by $\exp[-\mathrm{i}\frac{1}{2}\gamma G v t^2]$ before Fourier transformation. If necessary, signal/noise can be improved by addition of echoes in a truncated CPMG echo train provided, as discussed in the previous section, a magnitude operation is used before echo addition, to remove accumulated motion-induced phase shifts. Provided all samples are identical (such as jars of liquid baby food) a comparison of each profile with a standard profile serves to detect foreign bodies such as plastic or glass. Fig. 3A shows the profile of a bottle of pure water measured in the prototype sensor. Fig. 3B corresponds to the same sample except that a foreign body (a rubber bung) has been introduced. The foreign body is highlighted in the difference profile in Fig. 3C.

In principle, two-dimensional back-projection on-line imaging can be performed using only sample motion in fixed (non-switched) gradients if each echo in a CPMG echo train is acquired in a transverse gradient oriented at a progressively greater angle to the vertical. This on-line protocol has yet to be tested although the extended transverse gradient coils needed for this experiment have been designed (patent pending).

4.3. Single-shot on-line T_1 measurements

On-line, single-shot measurements of T_1 require special consideration because conventional sequences such as saturation or inversion recovery require repeated acquisition with step increases in the inversion or saturation recovery time. Fortunately the signal can be T_1-weighted either using polarisation contrast or by varying the degree of saturation with very rapid repeat acquisition on a timescale short compared to T_1 and the sample residence time in the RF coil.

For more direct single-shot on-line measurement of T_1 we have developed a novel pulse sequence called FIRE (for fast inversion recovery). This single-shot sequence shown in Fig. 4 actually measures both T_1 and T_2 and is similar to an inversion recovery sequence except that the signal is acquired not with an FID but with a truncated CPMG sequence of n-echoes. A 90_{-x} flip-back pulse on the $(n+1)$th echo of each truncated CPMG train then stores longitudinal magnetisation for a delay time t_1 before the next truncated CPMG sequence. The magnetisation eventually reaches a steady-state value that depends on both T_1 and T_2 so that fitting each CPMG echo train and the amplitude of the first echo of each truncated CPMG sequence gives both T_1 and T_2. Analytic expressions for extracting the relaxation times from the data are derived in the Appendix B. Fig. 5 shows the magnitude data for the FIRE sequence on a stationary 15% sucrose solution. Fitting the data gave a T_1 of 1600 ms, which can be compared with the more accurate, but slower Inversion Recovery value of 1976 ms. The FIRE sequence naturally tends to emphasise the short-time relaxation components in multiple exponential relaxation because there is insufficient time to acquire accurate baselines. Because of the non-exchanging CH protons and exchanging proton pool, the sucrose T_2 is actually biexponential with T_2's of 392 ms (7%) and 1735 ms (93%) so the FIRE value of 775 ms is an apparent value weighted on the shorter component. With a moving sample the number of inversion recovery steps (C1) and echoes (NECH) are limited by the sample residence time, though, as with the CPMG sequence, the sequence can be optimised by adjusting the RF pulse duration for each sample position in the RF coil and by using several RF coils positioned along the track. In the later case it is necessary to synchronise the pulse sequence so that only longitudinal magnetisation is transported between different RF coils during one of the C1 inversion recovery steps.

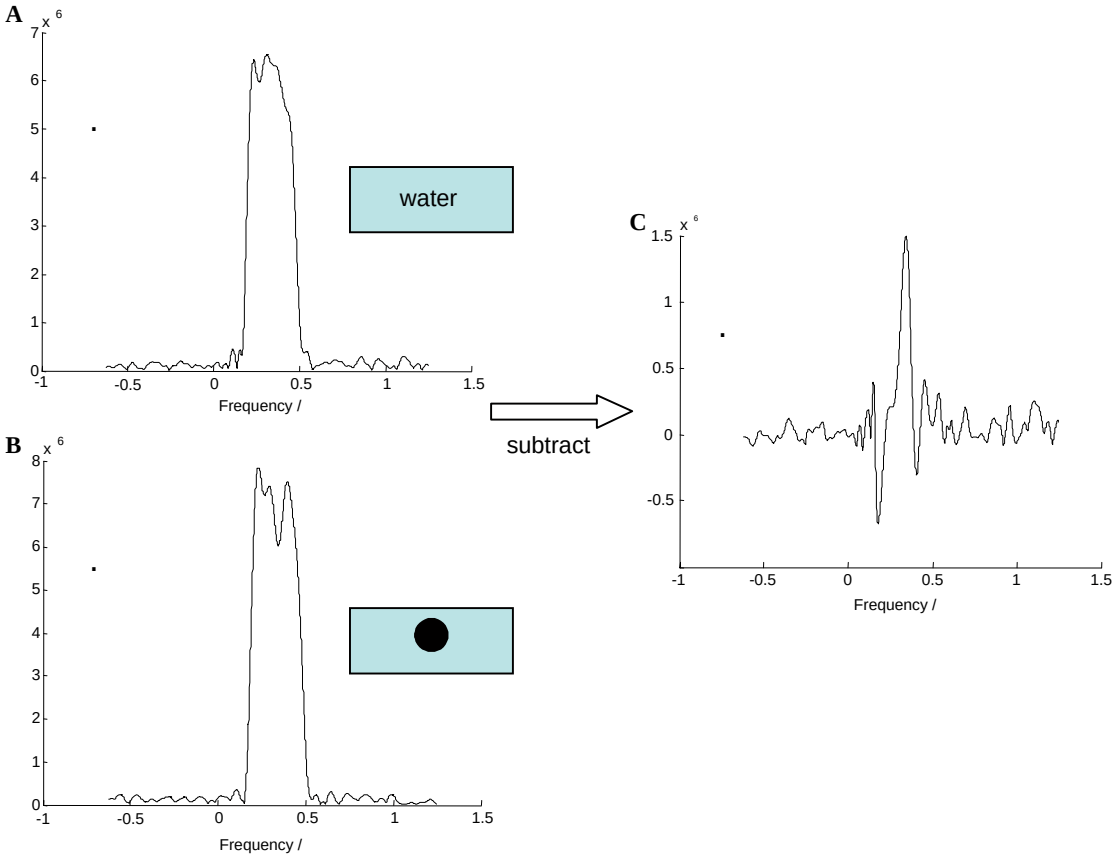

Fig. 3. One-dimensional image profiles acquired with the prototype on-line sensor. (A) A pure water sample. (B) Water with a foreign body (rubber bung). (C) The difference profile (A − B) highlighting the presence of the foreign body.

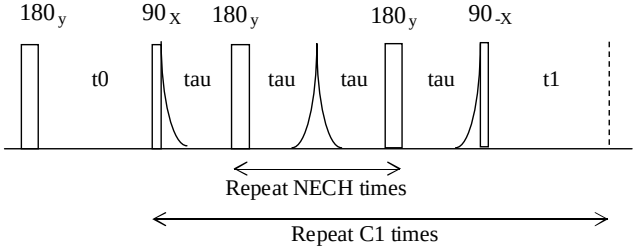

Fig. 4. The FIRE sequence for single-shot on-line measurement of T_1 (and T_2).

4.4. Single-shot on-line diffusion measurements

Consider the effect of translating a sample through a small region containing a local field gradient superimposed on top of the otherwise homogeneous solenoid B_0 field. If the direction of sample motion along the solenoid axis is labelled z, then even a non-linear gradient, G_z, oriented along the direction of sample motion does not cause dephasing because every spin in the sample will move through the whole of G_z and experience the same accumulated phase change. On-line diffusion measurements must therefore be done using localised transverse gradients, G_x or G_y and translation of the sample through the local, non-pulsed, transverse gradient is then motionally equivalent to applying a pulsed gradient on a stationary sample. Translational relaxation does, however, mean that longitudinal magnetisation and not transverse magnetisation must be conveyed between coils during the diffusion time. The simplest arrangement therefore mimics the pulsed gradient stimulated echo experiment and, in the pulsed RF mode, uses 2 RF coils and 2 constant-current transverse gradient coils, each gradient coil surrounding the RF coil (see Fig. 6). Passage through the first transverse gradient coil gives an accumulated phase twist characterised by the wavevector, q, where

$$q = \int \mathrm{d}z\gamma G_x(z)(z/v). \tag{18}$$

The second gradient coil reverses this dephasing twist and creates a motionally modified stimulated echo. Note especially that Eq. (18) implies that the gradient need not be a linear function of z, though it is necessary for it to be independent of (x, y) if meaningful diffusivities are to be measured. Unfortunately, in a single-shot sequence it is not possible to eliminate the effects of relaxation in the conventional way by taking the ratio of the stimulated echo amplitudes acquired with and without the gradient pulses. This on-line measurement will therefore only be of value for monitoring sample quality if diffusion is a more sensitive probe of sample quality than relaxation. The effect of

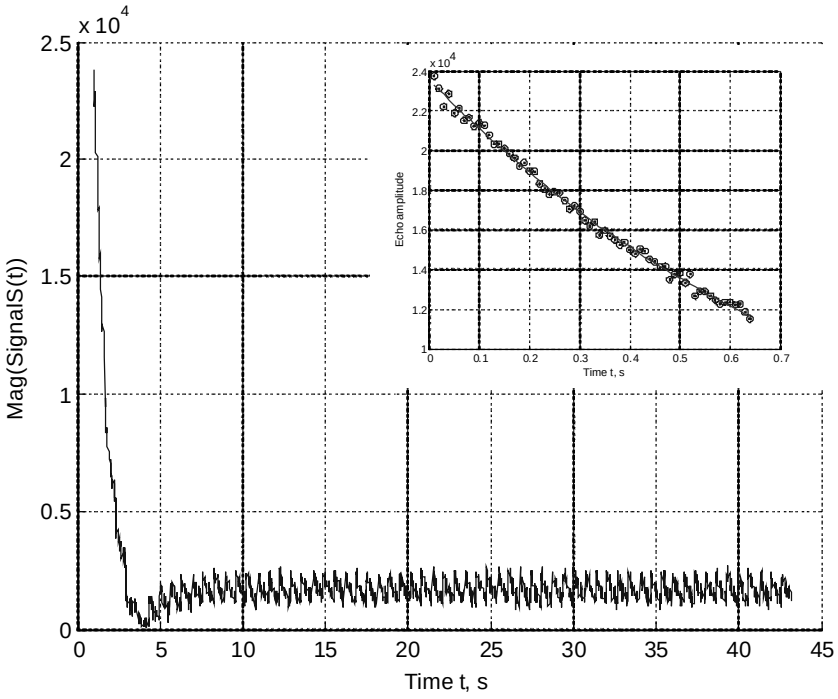

Fig. 5. Representative data for a 15% sucrose solution acquired with the FIRE sequence for single-shot, on-line T_1 and T_2 measurement. The saw-tooth structure arises from truncated CPMG echo trains, one of which is expanded and fitted in the inset.

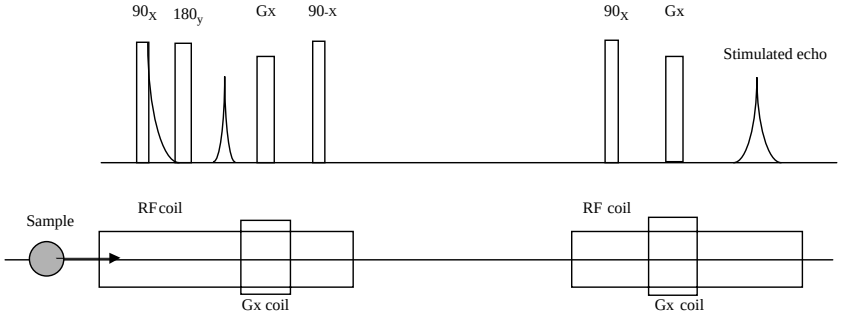

Fig. 6. Schematic of the single-shot on-line pulse sequence for diffusion and oil content determination.

variation in sample size on the stimulated echo amplitude needs to be taken into account when examining biological samples such as apples. This can be done by measuring the total magnetisation from the amplitude of the Hahn echo acquired in the first RF coil. Note especially that motional relativity means that it is not necessary to pulse the two transverse gradient coils. No expensive gradient amplifiers and programmers are therefore necessary, only low-cost constant-current power supplies.

4.5. Single-shot on-line oil content and BRIX determination

Because the effective water self-diffusion coefficient is usually much larger than that of oil, the pulse sequence shown in Fig. 6 can also be used for oil content determination by increasing the transverse gradient amplitudes to the point where the water signal is completely suppressed. The Hahn echo amplitude in the first RF coil then gives the total proton signal from both oil and water; whereas the stimulated echo amplitude arises only from oil. All that is then required is a linear calibration of the echo amplitude ratio verses oil content. We have already shown the feasibility of this protocol for determining the oil content of avocados using a commercial off-line spectrometer operating at 23.4 MHz and a stationary sample [4]. We have recently shown that a similar protocol can be used for the on-line determination of another important fruit quality factor, namely the soluble solid content (BRIX) value in fruit, which, is a recognised measure of the degree of ripeness (unpublished results).

5. Optimising on-line detection protocols

On-line NMR and MRI is still at an early stage of development and it is to be anticipated that sensitivity and signal quality can be improved by borrowing some of the pulse-

engineering strategies already developed in the NMR/MRI of stationary (or spinning) samples. We have already pointed out the potential for adjusting the phase and duration of each RF pulse in different locations along the conveyor track and this remains to be explored. However, even assuming the on-line pulse engineering or ST-equivalent can be perfected there remains the challenge of identifying the optimum on-line NMR acquisition protocol for detection of each quality factor for every type of sample of relevance to industry. In some applications, such as measurements of solid/liquid ratios or oil or water contents, the well-established off-line method can simply be transferred to the on-line situation. However, there are many, more subtle, quality factors where it is unclear which, if any, combination of NMR parameters, such as T_2, T_1 or D correlates with the quality defect. In such cases it is helpful to first explore the NMR parameter space with off-line multidimensional methods such as T_1–T_2 and T_2–D cross-correlation spectroscopy. To illustrate this strategy, consider the problem of the on-line detection of mealiness in apples, which is a serious industrial quality control problem that fails to get detected by existing on-line sensors. Mealiness results from a loss of cell adhesion within the tissue so that chewing merely separates the intact cells instead of liberating the intracellular juice. The first step in developing an on-line protocol for mealiness detection is therefore is to compare the two-dimensional T_1–T_2 correlation spectra [5–7] of healthy and mealy apples. A representative spectrum is reproduced in Fig. 7. Such spectra show whether longitudinal or transverse relaxation is the best probe of mealiness and whether short or long relaxation time components should be measured. In fact the data show that the short T_1 of peaks assigned to cell wall water become longer in mealy apples (unpublished results) which suggests that the on-line FIRE sequence might be able to discriminate degrees of apple mealiness, though this has yet to be tested on-line. Earlier off-line measurements at a higher field corresponding to 100 MHz showed that mealiness shortens the T_2^* of the main vacuolar water peak [8] (top right in Fig. 7) but this correlation is not observed at the low frequency used in the on-line system, confirming that it is a susceptibility-induced dephasing effect caused by increasing numbers of air spaces in the tissue. This illustrates how correlations established at high field may not be useful at the low fields used by commercially viable on-line NMR sensors.

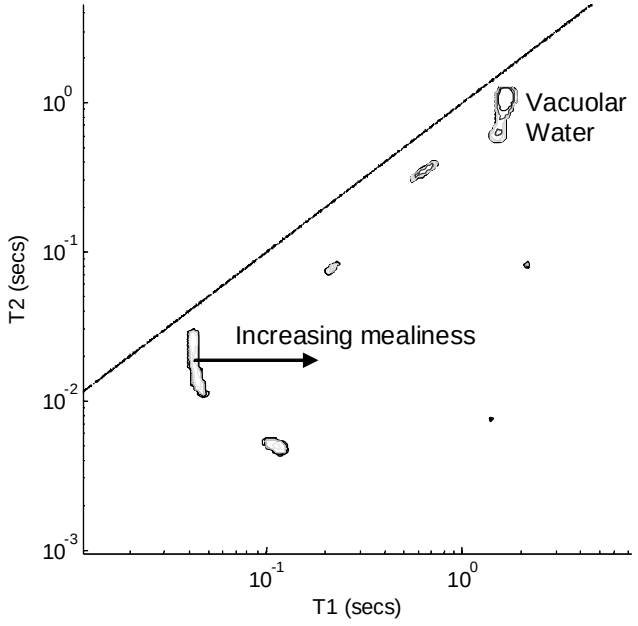

Fig. 7. A representative T_1–T_2 cross-correlation spectrum of a fresh red delicious apple acquired at 23.4 MHz with a 200 μs CPMG τ-spacing. The arrow indicates the shift in the water associated with the cell wall to longer T_1 with increasing mealiness.

6. Conclusions

Motional relativity presents several alternative ways of performing NMR that holds great promise for the eventual development of commercial, on-line NMR sensors. Cost is a major consideration if NMR technology is to find widespread application throughout the industrial sector and our combination of air-cooled solenoids and constant current field gradients means the sensor can be built for a fraction of the cost of existing off-line commercial NMR spectrometers or imagers. However, on-line NMR is still in its infancy and many aspects remain to be researched before the production of commercial units can be considered. These include the feasibility of the ST excitation mode and of two-dimensional back-projection imaging with constant (non-pulsed) gradients. The potentially exciting relationship between polarisation contrast and quality remains to be explored and this can be done by varying the number of polarising modules and their distance from the solenoid magnet. The possibility of RF-free excitation by translation through orthogonally oriented fields is another fascinating possibility to be explored.

It is worth bearing in mind that if the desired information on sample quality is contained in the surface layers then it is no longer necessary to use the solenoid magnet arrangement discussed in this paper. Instead passage of the sample over a one-sided magnet would be all that is necessary [13]. Of course, prepolarisation may still be necessary with long T_1 samples and the well-known problems of B_1 and B_0 field inhomogeneity in ex situ magnets need to be considered [14,15].

Sensitivity is another important issue that affects the commercial viability of any on-line NMR sensor. The example of foreign body detection illustrates this point. Although our results in Fig. 3 demonstrate the feasibility of on-line foreign body detection using only constant gradients, the detection limits in terms of size, shape, and orientation for different classes of foreign body have yet to be investigated and this aspect is critical to the sensor's commercial usefulness. Similarly the robustness of the NMR-quality correlations on moving samples in low fields remains to be researched with statistically significant

numbers of samples for industrially relevant problems. Many of the correlations reported in the literature between transverse relaxation rates and food quality only arise because of dephasing of the water signal by diffusion through internal gradients created by susceptibility differences across microscopic phase boundaries. This effect is important at high field [8] but is negligible at the low fields appropriate to on-line sensors. Similarly, transverse relaxation rates (and magnetisation transfer rates) in water-rich biological samples are strongly influenced by proton exchange between water and chemically shifted exchangeable protons on carbohydrate and amino acid moieties [9]. Because these chemical shift differences are field dependent, transverse relaxation rates in many biological samples are greatly reduced at low field. Similar considerations apply to longitudinal relaxation because the dispersive relation between T_1 and field strength generally means not only that T_1's are shorter at low frequencies but also that differences in T_1's resulting from differences in quality are also greater. Much work therefore remains to be done in establishing robust NMR-quality correlations at low field. The authors are currently working with a consortium of companies to research these various aspects.

Acknowledgments

The authors thank Niusa Marigheto for measuring the T_1–T_2 correlation spectra of fresh and mealy apples. The BBSRC is thanked for a grant under the SBRI scheme and a Link award from DEFRA is gratefully acknowledged. The assistance of the Resonance Instruments (now Oxford Instruments Molecular Biotools) in modifying the UltraMaran console; Dowding and Mills (Birmingham) for winding the solenoid coils; and Scipher International for incorporating the Eurotherm safety control system is gratefully acknowledged.

Appendix A. A computer simulation of the CPMG echo decay envelope for spherical samples moving through an off-centre, trapezoid RF coil in an inhomogeneous solenoid B_0 field

We assume, for simplicity, that the CPMG sequence is started with a 90_x pulse in the middle of the RF coil, so the initial, normalised magnetisation is simply along y in the rotating frame. However, the finite size of the RF coil means that as the sample moves through the coil it experiences a varying B_1 field. A pulse of sufficient duration to give a 180_y flip angle in the middle of the coil will only give a θ_y degree flip angle ($\theta < 180$) elsewhere in the coil if it is applied for the same duration. The B_1 field inhomogeneity can be characterised by the dependence of the flip angle, $\theta(z)$, on distance from the centre of the RF coil, z. For our transverse solenoid coil, $\theta(z)$ has an approximately trapezoid form because the centre part has a uniform B_1; whereas, because of the absence of the complete set of 45°-sloped coils, B_1 falls off linearly with z at the two ends. In the rotating frame the effect of a $\theta_y(z)$ pulse anywhere in the coil can be represented by the rotation matrix

$$\begin{pmatrix} \cos\theta(z) & 0 & -\sin\theta(z) \\ 0 & 1 & 0 \\ \sin\theta(z) & 0 & \cos\theta(z) \end{pmatrix}. \tag{A.1}$$

Free precession and relaxation during the time τ between $\theta(z)$ pulses can be simulated with the evolution matrix

$$\begin{pmatrix} \exp(-\tau/T_2)\cos\Delta\tau & \exp(-\tau/T_2)\sin\Delta\tau & 0 \\ \exp(-\tau/T_2)\sin\Delta\tau & \exp(-\tau/T_2)\cos\Delta\tau & 0 \\ 0 & 0 & \exp(-\tau/T_1) \end{pmatrix} \tag{A.2}$$

followed by addition of the term for longitudinal relaxation,

$$\begin{pmatrix} 0 \\ 0 \\ [1-\exp(-\tau/T1)] \end{pmatrix}. \tag{A.3}$$

In these expressions Δ is the resonance offset, which, because of B_0 inhomogeneity, depends on the location, z, of the spin in the magnet. In fact the resonance offset, $\Delta(z)$ is given as $[\gamma B(z)/2\pi - F]$ where F is the spectrometer frequency and $B(z)$ is the sensor field. $B(z)$ can be calculated analytically for most simple magnet geometries [11]. For an ideal solenoid magnet of length $2L$ and radius, R,

$$B(z) = B_0(\{\cos(\tan^{-1}[R/(L-z)]) + \cos(\tan^{-1}[R/(L+z)])\})/2\cos(\tan^{-1}(R/L)). \tag{A.4}$$

Because the sample is moving with velocity v, its position, z, at time t, is $(z_0 + vt)$ where z_0 is the position of an isochromat at time zero. These expressions can be used to calculate the echo amplitude for a sample of arbitrary profile along z. The simulation is greatly simplified if the phase change $\delta\varphi$, experienced by an isochromat in a time T can be calculated analytically. For the solenoid field it can be shown that

$$\begin{aligned} \delta\phi &= \int_0^T \mathrm{d}t\Delta(t) \\ &= 2\pi[FT - \{(\gamma B_0/2\pi)/2\cos(\tan^{-1}(R/L))\}\{I_+ + I_-\}], \end{aligned} \tag{A.5}$$

where

$$\begin{aligned} I_\pm &= \int_0^{\mathrm{T}} \mathrm{d}t\cos\{\tan^{-1}[R/(L \pm (z_0+vt))]\} \\ &= -(1/v) \pm [L^2 + R^2 \pm 2Lz_0 + z_0^2]^{1/2} \\ &\quad \pm (1/v)[L^2 + R^2 \pm 2LTv + T^2v^2 \pm 2Lz_0 + 2Tvz_0 + z_0^2]^{1/2}. \end{aligned} \tag{A.6}$$

Fig. 2A shows the z-dependence of B_0 for a solenoid of total length ($2L$) equal to 1.7 m and radius, R, 0.105 m. It also shows the B_1 field for a transverse tilted solenoid coil of total length 34 cm. The sample profile is a semi-ellipsoid corresponding to a sphere of diameter 7 cm. Fig. 2B shows

the CPMG echo decay envelopes calculated for this geometry for a set of velocities assuming that the 90° pulse coincides with the sample being in the centre of the RF coil.

Appendix B. Calculation of the echo amplitudes in the FIRE sequence

The FIRE pulse sequence is shown in Fig. 4. Let the magnetisation components at the start of the mth echo train ($m = 1,2,\ldots,c1$) immediately after the 90_x pulse which initiates the truncated CPMG sequence be written

$$M_x = 0; \quad M_y = M_{y,m}; \quad M_z = M_{z,m}. \tag{B.1}$$

After the first 90_x pulse of the $(m+1)$th CPMG train

$$M_{y,m+1} = M_0 - (M_0 - M_{y,m}\exp[-t/T_2])\exp(-t1/T_1), \tag{B.2}$$

where $t = 2(\mathrm{NECH}+1)\tau$. Gathering terms,

$$M_{y,m+1} = M_0(1-\beta) + \alpha\beta M_{y,m}, \tag{B.3}$$

where $\alpha = \exp(-t/T_2)$ and $\beta = \exp(-t1/T_1)$. By induction we deduce that

$$M_{y,n} = M_0(1-\beta)(1-\alpha^{n-1}\beta^{n-1})/(1-\alpha\beta) + \alpha^{n-1}\beta^{n-1}M_{y,1}. \tag{B.4}$$

But

$$M_{y,1} = M_0[1 - 2\exp(-t0/T_1)]. \tag{B.5}$$

Hence, the magnitude of the first echo in the nth CPMG train is

$$M_{y,n} = M_0\{[(1-\beta)(1-\alpha^{n-1}\beta^{n-1})/(1-\alpha\beta)] + (1 - 2\exp(-t0/T_1)\alpha^{n-1}\beta^{n-1})\}\alpha^2. \tag{B.6}$$

The factor α^2 takes account of transverse relaxation during the time $2t$. The asymptotic steady-state echo amplitude is seen to be

$$M_{y,\infty} = M_0\exp(-2\tau/T_2)[1-\exp(-t1/T_1)]/[1-\exp(-t1/T_1)\cdot\exp(-t/T_2)]. \tag{B.7}$$

References

[1] B.P. Hills, NMR detection of foreign bodies, in: M. Edwards (Ed.), Detecting Foreign Bodies in Food, Woodhead Publishing, Cambridge, 2004.

[2] B.P. Hills, C.J. Clark, Quality assessment of horticultural products by NMR, vol 50, in: Annual Reports on NMR spectroscopy, vol. 50, 2003, pp. 75–120.

[3] C.P. Slichter, Principles of Magnetic Resonance, Springer-Verlag/GmbH, Berlin and Heidelberg, 1989 (Chapter 2).

[4] N. Marigheto, S. Duarte, B.P. Hills, An NMR relaxation study of Avocado quality, Applied Magnetic Resonance (2005) in press.

[5] B.P. Hills, S. Benamira, N. Marigheto, K.M. Wright, T_1–T_2 correlation analysis of complex foods, Appl. Magn. Reson. 26 (2004) 543–560.

[6] Y.-Q. Song, L. Venkataramanan, M.D. Hurlimann, M. Flaum, P. Frulla, C. Straley, T_1–T_2 correlation spectra obtained using a fast two-dimensional Laplace Inversion, J. Magn. Reson. 154 (2002) 261–268.

[7] S. Godefroy, L.K. Creamer, P.J. Watkinson, P.T. Callaghan, The use of 2D Laplace inversion in food materials, in: P.S. Belton, A.M. Gil, G.A. Webb, D. Rutledge (Eds.), Magnetic Resonance in Food Science, The Royal Society of Chemistry, Cambridge, 2002, p. 85.

[8] P. Barreiro, A. Moya, E. Correa, M. Ruiz-Altisent, M. Fernandez-Valle, A. Peirs, K.M. Wright, B.P. Hills, Prospects for the rapid detection of mealiness in Apples by non-destructive NMR Relaxometry, Appl. Magn. Reson. 22 (2002) 387–400.

[9] B.P. Hills, Magnetic Resonance Imaging in Food Science, Wiley, New York, 1998.

[10] E.K. Jeong, D.H. Kim, M.J. Kim, S.H. Lee, J.S. Suh, Y.K. Kwong, A solenoid-like coil producing transverse RF fields for imaging, J. Magn. Reson. 127 (1997) 73–79.

[11] P. Lorrain, D.R. Corson, F. Lorrain, Electromagnetic Fields and Waves, W.H. Freeman Publishers, San Francisco, 1988.

[12] M.D. Mann, B.F. Chmelka, Measurement of dilute 29Si silicate species in solution using a large volume coil and DEFT NMR, Anal. Chem. 72 (2000) 5137–5145.

[13] B.P. Hills, Applications of low-field NMR to food science, in: G. Webb (Ed.), Annual Reports on NMR Spectroscopy, Academic Press, London (in press).

[14] M.D. Hurlimann, Diffusion and relaxation effects in general stray field NMR experiments, J. Magn. Reson. 148 (2001) 367–378.

[15] M.C.A. Brown, D.A. Verganelakis, M.J.D. Mallett, J. Mitchell, P. Blumler, Surface normal imaging with a hand-held NMR device, J. Magn. Reson. 169 (2004) 308–312.